Solubility of hydrogen at low concentrations in thin epitaxial Nb(110) films

2004 J. Phys.: Condens. Matter 16 1165

(http://iopscience.iop.org/0953-8984/16/8/002)

INSTITUTE OF PHYSICS PUBLISHING JOURNAL OF PHYSICS: CONDENSED MATTER

J. Phys.: Condens. Matter **16** (2004) 1165–1174 PII: S0953-8984(04)72925-2

Solubility of hydrogen at low concentrations in thin epitaxial Nb(110) films

Emil Johansson[1], **Stefan Olsson, Cyril Chacon and Björgvin Hjörvarsson**

Department of Physics, Uppsala University, Box 530, S-751 21 Uppsala, Sweden

E-mail: emil.johansson@fysik.uu.se

Received 3 December 2003
Published 13 February 2004
Online at stacks.iop.org/JPhysCM/16/1165 (DOI: 10.1088/0953-8984/16/8/002)

Abstract

Hydrogen absorption of thin epitaxial Nb(110) films have been studied by x-ray diffraction and *in situ* four-probe resistivity measurements. The hydrogen absorption at low concentrations is strongly affected by the thickness of the Nb films and for the two thinnest films a temperature dependence in the absorption potential is observed. The difference in solubility is linked to changes in the average cell volume, which scales with the inverse film thickness. Clear concentration gradients in Nb films can be observed. The presence of multiple absorption energies is shown to limit the possibility to obtain relevant absorption and interaction potentials by conventional Sievert's and van't Hoff analysis.

(Some figures in this article are in colour only in the electronic version)

1. Introduction

The hydrogen absorption of bulk materials is well known [1] and is often referred to as a model system for the lattice gas model [2]. Development of the growth of high quality thin films and superlattices has created possibilities for exploring new aspects of hydrogen uptake, namely, the finite size and strain effects. Epitaxial Nb and V have served as model systems in this context [3–9]. Miceli *et al* [3] were the first to demonstrate the one-dimensional hydrogen-induced expansion. The influence of the unusually strong adhesion to the substrate, often referred to as clamping, was further elaborated by Steiger *et al* [5] in their investigations of hydrogen uptake in thin niobium films using the $^{1}H(^{15}N, \alpha\gamma)^{12}C$ nuclear resonance reaction. A strong reduction in the H–H interaction was inferred, originating from adhesion to the substrate. The finite size effects of the hydrogen interaction were further explored by Song and coworkers [6] via *in situ* XRD (x-ray diffraction) measurements on epitaxial Nb(110) films with thicknesses ranging from 300 to 5200 Å. The measured isotherms were well described by the standard expression of solubility for a monatomic lattice gas which reduces to the

[1] Author to whom any correspondence should be addressed.

well known Sievert's law at low concentrations [5]. Besides clamping effects on the H–H interaction energy they found a large influence of the film thickness on the maximum relative lattice expansion.

Here we address the hydrogen uptake of thin epitaxial Nb(110) films at extremely low hydrogen concentrations. We will dwell on the influence of film thickness and misfit dislocations in Nb(110) on the initial stages of absorption and discuss the applicability of Sievert's law and van't Hoff analysis. For extremely thin layers, the Nb(110) lattice can be regarded as an extension of the Al sub-lattice in $Al_2O_3(11\bar{2}0)$ where the lattice mismatch is compensated for by straining the Nb layer (clamping) [10–12]. Close to defect-free growth of Nb is possible up to a certain film thickness, often referred to as the critical thickness (L_c). Above this critical thickness, the strain energy is reduced by forming misfit dislocations. Using a simple expression developed by Matthews *et al* [13], Grier and co-workers [12] estimated this thickness for Nb(110) on $Al_2O_3(11\bar{2}0)$ to be approximately 72 Å. Generally, hydrogen absorption is more favourable in vacancy-rich regions [14] and the impact of misfit dislocations on the hydrogen uptake should therefore be pronounced when the film thickness is comparable with the critical thickness. This is further addressed in the forthcoming pages.

2. Experimental details

2.1. Sample growth and structural characterization

The Nb(110) samples were prepared by molecular-beam epitaxy on $Al_2O_3(11\bar{2}0)$ substrates. The substrates were solvent cleaned and loaded in the ultra-high-vacuum chamber and annealed for 36 h at 1023 K. The base pressure in the chamber was typically in the 10^{-11} mbar range. Nb was evaporated from a multi-pocket electron gun with a growth rate of 0.5 Å s^{-1}. A capping layer of Pd was evaporated on top of the films, serving both as a catalyst for hydrogen dissociation and an oxidation barrier [15]. For further details about the growth of Nb films see, for example, Durbin *et al* [16].

The thicknesses of the samples were determined by x-ray reflectivity measurements using a Philips PW 3020 with Cu Kα-radiation and a scintillation detector. A Bruker D5000 equipped with a graphite monochromator, divergence, anti-scatter and Soller slits was used to establish the crystalline quality and the mosaicity of the films. Both θ–2θ ($2\theta = 37°-42°$) and ω scans were performed around the Nb(110) reflection, before and after hydrogen exposure. The width of the Lorentzian component in the ω scans is limited by the angular resolution of the instrument, which was of the order of 0.009°.

2.2. Solubility measurements

The solubility isotherms were established by applying *in situ* four-probe resistivity measurements using a Stanford Research 830 lock-in amplifier and recording the resistivity change during hydrogen loading and unloading. Details concerning the experimental set-up have been described before (see, for example, [17]) and therefore only a brief description will be given here. The temperature of the sample was controlled and monitored by a Eurotherm 94c temperature controller using a type K (chromel–alumel) thermocouple with an accuracy of 1 K. Pressure reading was performed by a CCM capacitance manometer (0–133 mbar) with an accuracy of 0.1% of full scale. The hydrogen gas, 99.9996% purity, used in the experiments was additionally purified in two steps: initially by using a West Associates ULTRAPURE gas purifier and thereafter by absorption/desorption in a metal-hydride storage bed. Prior to the measurements, the complete system, including the sample holder, was evacuated to a pressure

below 10^{-8} mbar. While pumping, the main contribution to the residual gas, as determined by a quadrupole mass spectrometer, is hydrogen. The P–$\frac{\Delta R}{R_0}$ isotherms, where R_0 is the resistance without hydrogen at 548 K, were measured by a stepwise increase of the hydrogen pressure at fixed temperatures. All the sequences started with the highest temperature. Four isotherms were measured, in steps of 25 K, in the interval 548–623 K. The temperature range was chosen in order to measure the isotherms well above the critical point for phase transformation, $\alpha \rightarrow \alpha'$ ($T_c = 444$ K in bulk) [18]. After completing the isotherms, the hydrogen was evacuated and the system, including the sample stage, was degassed while pumping for a minimum of 12 h.

The change in resistivity due to hydrogen uptake in bulk Nb can be approximated by a linear dependence at low concentrations. At higher concentrations the resistivity change involves a quadratic term [19]. Here we use the following approach, developed in [8, 17, 20], to ensure as accurate a determination as possible in the analysis:

$$C \approx C(\Delta R_{\max}) - C(\Delta R_{\max})\sqrt{1 - \frac{\Delta R}{\Delta R_{\max}}} \tag{1}$$

where $C(\Delta R_{\max})$ is the hydrogen concentration at maximum resistivity change which corresponds roughly to the half-filling of the available sites ($C = 50$ H/M%). $\Delta R_{\max}$ was determined when all solubility and initial XRD measurements were completed, as the exposure to high hydrogen pressures (high concentration of H) can affect the structural coherence of the lattice. Resistivity measurements only provide an indirect method to determine the hydrogen concentration in thin films and a conversion of ΔR to C using equation (1) will always suffer from uncertainties in the calibration procedure. However, while measuring the concentrations at elevated temperatures where the hydrogen is in a disordered state, the precision of the measurements are almost solely determined by the resolution of the measurements.

2.3. Hydrogen depth profiling

The N-15 method was used for performing the depth profiling [21] of hydrogen in the samples, at the Tandem accelerator in Uppsala. The technique is based on the ^{1}H(^{15}N, $\alpha\gamma$)^{12}C nuclear resonance reaction, in which the hydrogen depth profile as well as the total amount of hydrogen is determined. When performing hydrogen profiling, the sample is bombarded by ^{15}N ions with an energy equal to or above the resonance energy (6.385 MeV). Upon penetration, the ions lose energy and, at a depth at which the ions have the resonance energy, the probability for the reaction is greatly enhanced. The depth resolution is about some 10 Å close to the surface, but deteriorates with increasing depth, due to energy straggling. The detection limit is typically some atomic ppm and the precision is determined by the counting statistics. The accuracy is typically governed by the calibration standard and the accuracy in the stopping powers. The samples used in the profiling experiment were without Pd capping. An oxide layer is formed at the surface, which effectively hinders desorption of hydrogen while transport and measurements take place. The depth profiling was performed at room temperature.

3. Results and discussion

3.1. Structural characterization

The ω scans of all the investigated films exhibited two components, characteristic for high quality epitaxial Nb(110)-films [22]. The FWHM (full width at half-maximum) of the sharp and broad component were typically 0.03° and 0.15°, respectively.

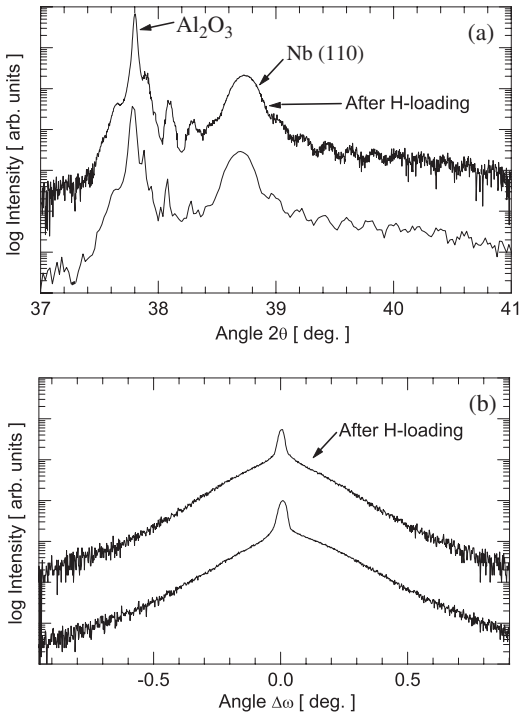

Figure 1. (a) θ–2θ and (b) rocking curve measurements, before and after hydrogen loading for the Nb film with a thickness of 539 Å. The full width at half-maximum of the rocking curve before H-loading is 0.032° and 0.14° and after H-loading it is 0.03° and 0.15° for the Lorentzian and Gaussian components, respectively.

Examples of θ–2θ and ω scans around the Nb(110) peak, before and after hydrogen loading, are illustrated in figures 1(a) and (b) and the most relevant structural parameters are found in table 1. A small systematic change in the average lattice spacing with film thickness is apparent from these analysis. The influence of strain state and clamping on hydrogen uptake is pronounced [5] and hence effects from the relaxation might be expected in the thermodynamic properties of the films. As seen in figure 1(b) and table 1, the hydrogen loading only modestly reduces the structural quality in the thickest film (1009 Å). However, as even small structural changes can have a large impact on the hydrogen uptake, through the H-vacancy interactions, these changes have to be considered later in the discussion. The change in coherency in the thinner films was within the uncertainty of the measurements. However, a small systematic reduction of the FWHM of the Lorentzian component of the Bragg peak appears to be present. An increased coherence length through cold annealing can account for such changes [22, 23]. The occurrence of misfit dislocations in Nb(110) on $Al_2O_3(11\bar{2}0)$ has been observed by previous transmission electron microscopy studies [10–12]. Nb(110) can grow epitaxially, with low defect density on a $Al_2O_3(11\bar{2}0)$ substrate, up to a critical thickness. Misfit dislocations are readily formed when the film thickness exceeds L_c, as previously discussed. Grier *et al* [12] estimated L_c, using the Matthews–Blakeslee approach [13], to be approximately 72 Å.

In this paragraph we use a discrete model describing the changes of the lattice parameter with film thickness. We divide the film into two regions with different cell volumes, as illustrated in figure 2. This approach is legitimized by the simplicity and the correct

Table 1. Average out-of-plane lattice spacing parameter, $\bar{d}(110)$, and full width at half-maximum of the ω scan before and after hydrogen loading. The values within brackets denote the maximum error in the last digit.

L (Å)	$\bar{d}(110)$ (Å)	ω scan, FWHM (deg)			
		a	b	c	d
1009	2.3266(2)	0.017(4)	0.028(5)	0.062(1)	0.126(1)
539	2.3261(4)	0.032(3)	0.030(7)	0.147(5)	0.15(1)
309	2.3206(2)	0.030(4)	0.026(9)	0.15(1)	0.10(5)
215	2.3184(7)	0.033(5)	0.020(9)	0.16(2)	0.19(4)

[a] Lorentzian component before hydrogen loading.
[b] Lorentzian component after hydrogen loading.
[c] Gaussian component before hydrogen loading.
[d] Gaussian component after hydrogen loading.

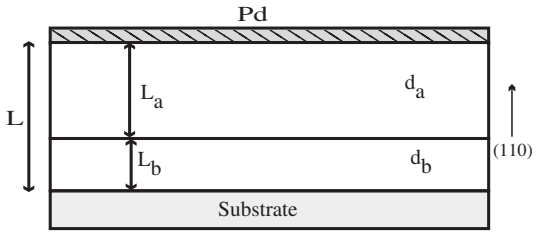

Figure 2. Schematic illustration of the different regions in the Nb films. L is the total thickness and d_a and d_b represent the out-of-plane lattice spacings in each region.

asymptotic description of the lattice parameter. However, we have to emphasize the imposed oversimplification. After the onset of defect formation, the misfit relaxation is close to a continuous process, due to the large number of defects/unit area, and not a step function. The variation in lattice parameter and the description of the changes in the absorption potential are still essentially the same. By using the discrete-two-region model, the observed (110) lattice spacing should decrease linearly with $1/L$, when $L \geqslant L_b$:

$$\bar{d} = d_a + \frac{L_b \Delta d}{L} \tag{2}$$

where d_a is the atomic plane spacing of the outermost region, L_b is the thickness of the near-substrate region, Δd is the difference between the two out-of-plane spacings $[d_b(110) - d_a(110)]$ and L is the total film thickness ($L = L_a + L_b$). The observed (110) spacing will decrease continuously with the inverse film thickness and reach a constant value when $L \leqslant L_b$, according to this description, which yields the same asymptotic behaviour as a continuous decrease with a cut-off value.

We can test the applicability of this model by performing a simple analysis of the parameters obtained. In figure 3 the average out-of-plane lattice spacing, $\bar{d}(110)$, is plotted as a function of the inverse film thickness. Apparently, $\bar{d}$ scales linearly with $1/L$ and converges to the bulk value [24] as $1/L \to 0$. Relaxation of the misfit strain between the substrate and the film is therefore evident, as the film thickness increases. The slope in figure 3 is determined to be -2.4 Å^2. By using the estimated strain in the (110) direction ($\approx 0.4\%$) as an upper value, the thickness of the layer L_b is estimated to be <260 Å (slope $= \Delta d L_b$). This conclusion is consistent with the results of Grier *et al* [12], as the critical thickness for the formation of misfit dislocations must be smaller than the thickness required for establishing unstrained

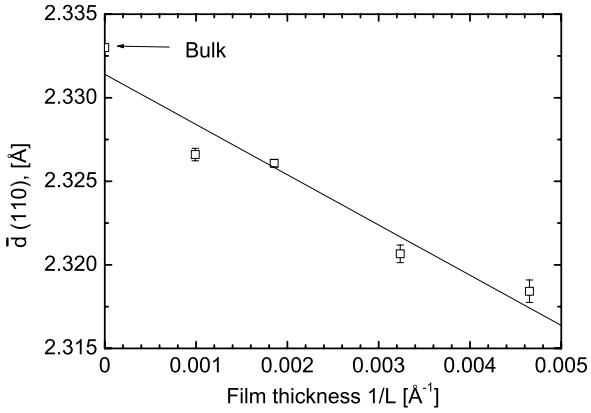

Figure 3. Variation of the average (110) plane lattice spacing with inverse film thickness. The full line represents the linear fit.

growth ($L_c \ll L_b$). The extension of the region by varying the lattice parameter is thus in the same range, as the films discussed here. Therefore, as the hydrogen uptake reflects the changes in the lattice parameter, the influence of these variations should be relatively easy to observe, as will be shown in the next section.

3.2. Solubility isotherms and thermodynamic analysis

The measured hydrogen absorption P–C isotherms for the Nb(110) thin films are presented in figures 4(a)–(d) as Sievert's plots. The value from the literature for H in bulk Nb, at 623 K, is included as a comparison [25]. The solubility in the films is smaller than in bulk Nb, in agreement with previous investigations [3, 5]. At first glance, the solubility increases with increasing film thickness, in line with previous studies, see, for example, Steiger *et al* [5] and Miceli *et al* [3], The 1009 Å thick film is an exception as the solubility for this thickness is higher than in the 539 Å film. As stated earlier, the thickest sample showed pronounced structural deterioration upon hydrogen exposure and the results might therefore not represent the thermodynamic properties of the as-grown film. All further comparisons between these films have therefore to be made with caution.

At first sight, all the films exhibit Sievert's-like uptake for concentrations up to 4 H/Nb%, i.e.

$$\sqrt{P} = K_s C \tag{3}$$

where P is the external hydrogen pressure, K_s is the Sievert constant and C is the hydrogen concentration in the film. When taking a closer look into the low concentration region (0–1%), as illustrated in figure 5, it becomes clear that the uptake in the two thinnest films is noticeably different, as compared to the thicker ones. Sievert's law appears not to be applicable for concentrations above 0.7 H/Nb% in those films (215 and 309 Å). Instead, these samples exhibit two clearly distinguishable linear regions: one when H/Nb $\lesssim$ 0.7%, followed by a second linear region for 0.7 $\lesssim$ H/Nb $\lesssim$ 4%, both with intercepts through zero but with different slopes (see figure 5).

The presence of a temperature dependence is readily explored. First we calculate the expected pressure at H/Nb $\leqslant$ 0.7%, using the data from 1 $\leqslant$ H/Nb $\leqslant$ 4%. The difference between this pressure and the one obtained ($\Delta\sqrt{P}$) is plotted at a given concentration. The results for H/Nb = 0.65% are displayed in figure 6. A clear temperature dependence is

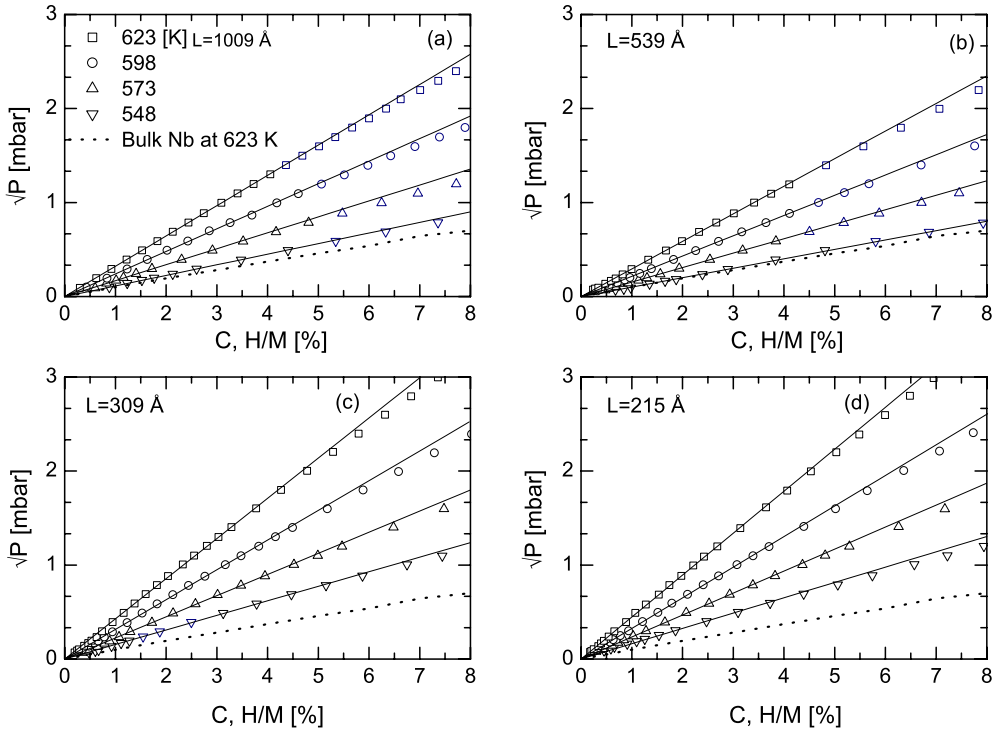

Figure 4. (a)–(d) Variation of the square root of pressure with hydrogen concentration at constant temperatures for Nb(110) films on a sapphire substrate. P is the applied hydrogen pressure and C is the concentration of the hydrogen absorbed in the film. The symbols representing the different temperatures are the same in all graphs. The full lines represent the fits in the concentration region 0–4 H/Nb% and is just a guide for the eye at higher concentrations. To illustrate when H–H interactions no longer can be neglected data for $C \geqslant 4$H/Nb% are included. The bulk data come from [25].

revealed, which can lead to severe misinterpretation when trying to separate the chemical potential in enthalpy and entropy terms: the standard way to determine $\Delta H_{\mathrm{H}}^{0}$ and $\Delta S_{\mathrm{H}}^{0}$ by using the slope and intercept of a plot of $\ln K_{\mathrm{S}}$ versus $1/T$ is only applicable if the enthalpy and entropy is temperature-independent. The inability to separate in enthalpy and entropy terms will also, consequently, lead to problems when trying to determine the variation of the different quantities with concentration from the van't Hoff equation. The reason for the unusual temperature dependence can be the occurrence of multiple absorption sites with energy differences comparable to $k_{\mathrm{B}}T$.

The picture of multiple absorption sites in the Nb films is also supported by the dependence of the solubility on the film thickness, see figures 4 and 5. The difference in solubility must therefore be reflected in different concentrations at different depths. This possibility was investigated at the Tandem accelerator in Uppsala by using the $^{1}\mathrm{H}(^{15}\mathrm{N}, \alpha\gamma)^{12}\mathrm{C}$ nuclear resonance analysis (NRA) [26]. The profiling was performed on a 50 nm Nb film, without any Pd capping, to hinder desorption of H during the measurements. The film was initially loaded at 500 K, cooled down to 298 K and thereafter moved to the accelerator in ambient air. A thin oxide layer is formed on the Nb(110) surface, effectively blocking the uptake and release of hydrogen [27]. The measurements were performed at ambient temperature. A typical depth profile is shown in figure 7, where we plot the number of gamma counts/microcoulomb

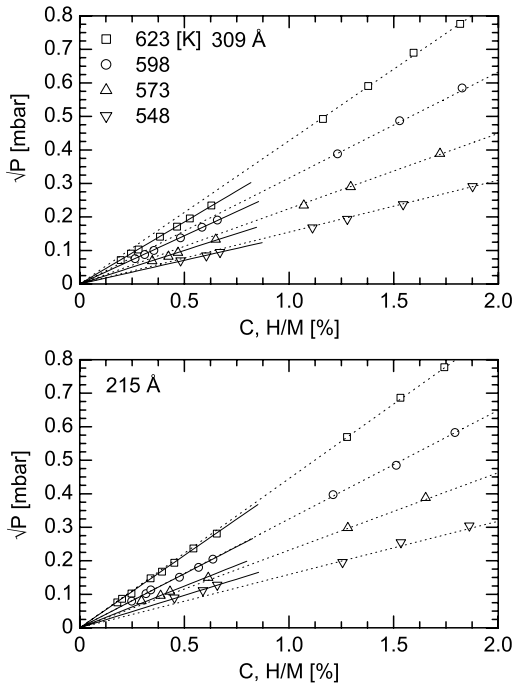

Figure 5. Variation of the square root of pressure at low hydrogen concentrations for the 309 and 215 Å films. The full and broken lines represent the linear fits for each region.

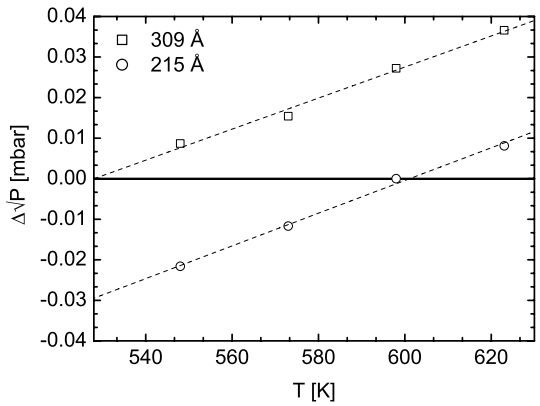

Figure 6. Variation of the square root of pressure at low hydrogen concentrations for the 309 and 215 Å films. The broken lines represents the linear fits.

(doze) as well as the deduced hydrogen concentration. As seen in the figure, the presence of a concentration gradient is evident, reflecting the changes in solubility, as expected from the discussion above. At low concentrations, the hydrogen resides preferentially close to the surface, consistent with the thickness dependence of the solubility. At the lowest concentrations, the hydrogen depth profile reflects the initial potential, influenced by the strain state as well as the defect profile of the sample. The same conclusion can be drawn from the results of Steiger *et al* [5]. They also observed clear evidence for a concentration gradient

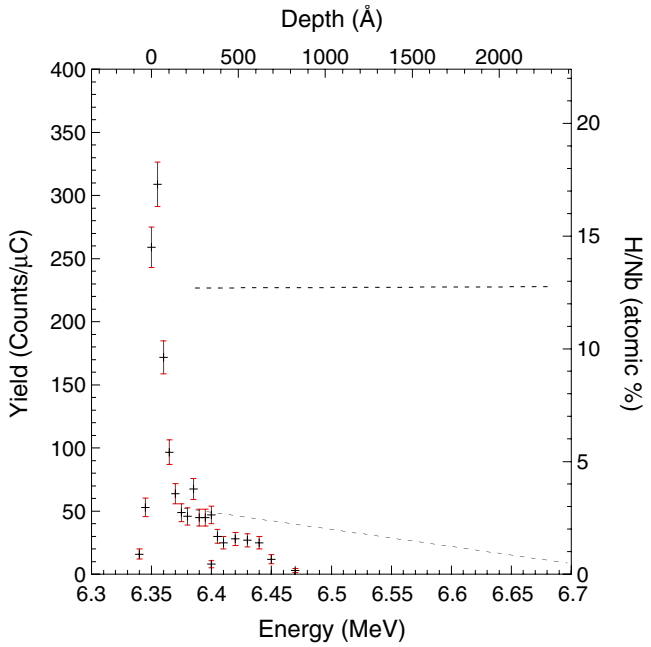

Figure 7. Hydrogen depth profiling of a 500 Å Nb(110) sample. The broken lines illustrate the results from [5] for a 1430 Å thick film. The high concentration in the near-surface region originates from the presence of H-containing species adsorbed at the surface.

at a hydrogen concentration around 1 at.%, with the lowest concentration at the Nb/Al_2O_3 interface. When the total concentration was increased (not shown here), the concentration gradient diminished and finally reversed at concentrations around 0.5 in H/Nb. Furthermore, the region with lower solubility decreases with respect to the total volume of the absorbing film when the film thickness is increased. Thus, a consistent view on the observed variation in the solubility emerges.

These results clearly demonstrate the complexity of the hydrogen absorption potential in Nb thin films. The use of a single site absorption potential and spatially invariant interaction energy must therefore be questioned in this context.

4. Summary and conclusions

Hydrogen solubility isotherms in epitaxial Nb(110) films have been measured by using *in situ* four-probe resistivity measurements. The solubility is shown to exhibit strong thickness dependence at low concentrations and a temperature dependence in the population in the thinnest films is evident. The change in the absorption potential originates in the change of cell volume with film thickness. A discrete step model is used to describe the changes and an effective thickness of the layer closest to the substrate is determined to be approximately 260 Å. This model is a gross simplification of the variation of strain relief but catches the essence of the change in lattice volume and hydrogen solubility.

The results are consistent with previous studies of the thickness-dependent defect generation [12]. The solubility increases with film thickness, except for the thickest film (1009 Å). This deviation is accompanied with irreversible changes in the crystal quality, not seen in the thinner films. The critical concentration for hydrogen-induced defect generation

decreases with increasing film thickness. The restoring force from the substrate is constant and the energy available for defect generation increases linearly with thickness at a given concentration. Irreversible self-modifications of the H absorption potential has therefore to be carefully considered.

Deviations from Sievert's behaviour is observed in the thinnest films at low concentrations, consistent with the presence of more than one absorption energy. In addition, clear concentration gradients are observed. At the lowest concentrations, the region close to the substrate contains the smallest amount of hydrogen and the concentration increases close to linearly with increasing distance from the oxide interface. As the elastic interaction is closely related to volume change, the spatial variation in the interaction energy might be responsible for the thickness dependence of the hydrogen-induced expansion in Nb films [28].

A full description of the absorption process requires the use of multiple absorption sites with variable interaction energies. The concentration profile has to be known at different concentrations and temperatures in order to determine the parameters correctly describing the uptake.

Acknowledgments

The authors would like to thank Dr Joseph Bloch for valuable discussions. This project was financially supported by The Swedish National Energy Administration and the Swedish Research Council.

References

[1] Schober T and Wenzl H 1978 *Hydrogen in Metals II* (*Springer Topics in Applied Physics* vol 29) ed G Alefeld (Berlin: Springer) chapter 2, p 11
[2] Fukai Y 1993 *The Metal–Hydrogen System* (*Springer Series in Materials Science* vol 21) (Berlin: Springer)
[3] Miceli P F, Zabel H and Cunningham J E 1985 *Phys. Rev. Lett.* **54** 917
[4] Hjörvarsson B, Ryden J, Karlsson E, Birch J and Sundgren J E 1991 *Phys. Rev.* B **43** 6440
[5] Steiger J, Blässer S and Weidinger A 1994 *Phys. Rev.* B **49** 5570
[6] Song G, Geitz M, Abromeit A Q and Zabel H 1996 *Phys. Rev.* B **54** 14093
[7] Reisfeld G, Jisrawi N M, Ruckman M W and Strongin M 1996 *Phys. Rev.* B **53** 4974
[8] Olsson S, Blomqvist P and Hjörvarsson B 2001 *J. Phys.: Condens. Matter* **13** 1685
[9] Olsson S, Hjörvarsson B, Svedberg E and Umezava K 2002 *Phys. Rev.* B **66** 155433
[10] Gutekunst G, Mayer J and Rühle M 1997 *Phil. Mag.* A **75** 1329
[11] Gutekunst G, Mayer J, Viter V and Rühle M 1997 *Phil. Mag.* A **75** 1357
[12] Grier E J, Jenkins M L, Petford-Long A K, Ward R C C and Wells M R 2000 *Thin Solid Films* **358** 94
[13] Matthews J and Blakeslee A 1974 *J. Cryst. Growth* **27** 118
[14] Besenbacher F, Nielsen B B, Norskov J, Meyers S and Nordlander P 1990 *J. Fusion Energy* **9** 257
[15] Pick M A, Davenport J W, Strongin M and Dienes G J 1979 *Phys. Rev. Lett.* **43** 286
[16] Durbin S M, Cunningham J E, Mochel M E and Flynn C P 1981 *J. Phys. F: Met. Phys.* **11** L223
[17] Stillesjö F, Olafsson S, Isberg P and Hjörvarsson B 1995 *J. Phys.: Condens. Matter* **7** 8139
[18] Smith J F 1983 *Bull. Alloy Phase Diag.* **4**
[19] Watanabe K and Fukai Y 1980 *J. Phys. F: Met. Phys.* **10** 1795
[20] Andersson G, Hjörvarsson B and Zabel H 1997 *Phys. Rev.* B **55** 15905
[21] Lanford W, Trautvetter H, Ziegler J and Keller J 1976 *Appl. Phys. Lett.* **28** 566
[22] Wildes A, Mayer J and Theis-Bröhl K 2001 *Thin Solid Films* **401** 7
[23] Reimer P M, Zabel H, Flynn C P and Dura J A 1992 *Phys. Rev.* B **45** 11426
[24] Ashcroft N W and Mermin N D 1976 *Solid State Physics* (Philadelphia, PA: Saunders)
[25] Veleckis E and Edwards R K 1969 *J. Phys. Chem.* **73** 683
[26] Hjörvarsson B 1990 *PhD Thesis* Uppsala University, Uppsala, Sweden
[27] Hellwig O and Zabel H 2000 *Physica* B **283** 228
[28] Miceli P F, Zabel H, Dura J A and Flynn C P 1991 *J. Mater. Res.* **6** 964